

Stiction, Adhesion Energy and the Casimir Effect in Micromechanical Systems

E. Buks and M. L. Roukes

Condensed Matter Physics, California Institute of Technology, Pasadena, CA 91125

(December 2, 2024)

We measure the adhesion energy of gold using a micromachined cantilever beam. Stress and stiffness of the beam are characterized by measuring the spectrum of mechanical vibrations and the deflection due to external force. We induce stiction between the beam and a nearby surface employing capillary forces to determine the adhesion energy. The obtained value $\gamma = 0.06 \text{ J/m}^2$ is a factor of six smaller than the one predicted by idealized theory. This discrepancy may arise from surface roughness or an adsorbed layer intervening between the contacting surfaces in these mesoscopic structures.

PACS numbers: 68.10.Cr, 68.35.Gy, 87.80.Mj

The Casimir effect [1] is one of the most striking consequences of quantum electrodynamics (for a recent review see [2]). The dependence of the ground state energy of the electromagnetic field upon boundary conditions gives rise to an observable force between macroscopic bodies. A significant enhancement in the accuracy of measuring the Casimir force has been achieved recently with experiments employing torsion pendulum [3] and atomic force microscope (AFM) [4]. Casimir effect investigations may open the way for experimental observation of new fundamental forces arising from the hypothetical extra dimensions predicted by modern theories (see for example [5]). However to enable such studies it is crucial to improve experimental techniques. The Casimir force, in addition to its fundamental interest, also plays an important role in the fabrication and operation of micro electromechanical systems (MEMS). This technology allows fabrication of variety of on-chip fully integrated sensors and actuators with rapidly growing number of applications. One of the principal causes of malfunctioning in MEMS is *stiction*, namely collapse of movable elements into nearby surfaces, resulting in their permanent adhesion (for a review see [6], [7]). This can occur during fabrication, especially due to capillary forces present during drying of a liquid from the surface of the sample, or during operation. It was argued recently that the Casimir effect is often an important underlying mechanism causing this phenomena [8].

Here we report our experimental study of surface-surface interactions using micromachined Au cantilevers. In particular, we focus upon the extreme manifestation of the Casimir interaction, namely, adhesion between surfaces and the associated energy of this process. The structures we use are designed to allow straightforward and unambiguous interpretation of our results. We use bulk micromachining (rather than surface micromachining), in which the substrate is completely removed beneath the sample. This greatly simplifies the boundary conditions of the electromagnetic field in the vicinity of the sample. Moreover, we avoid using multi-layered structures, since their internal stresses generally play an

important role and theoretical modeling is thus more difficult. We use metallic rather than semiconductor structure to minimize the possibility of parasitic bound surface charge attraction.

After characterizing the mechanical properties of the beam, we induce stiction between the beam and a nearby electrode. The shape of the beam after adhesion and the elastic energy associated with this configuration allow us to determine the attractive surface energy. Similar methods were employed to measure the adhesion energy of stress-free Si [6], [7]. Note however that generally mechanical properties such as stress have to be characterized in order to accurately determine the elastic energy. We conclude by comparing our results with previous measurements and with theory.

The bulk micromachining process employed for sample fabrication is described in Fig. 1. In the first step chemical vapor deposition is employed to deposit 70 nm thick layer of Si_3N_4 on front and back sides of a Si wafer. A square window is opened in the Si_3N_4 on the back using photolithography and wet etching (Fig. 1(a)). The high selectivity and anisotropic etching properties of KOH are employed to form the structure shown in Fig. 1(b), with a $300\mu\text{m}$ square of Si_3N_4 suspended membrane on the front side of the wafer. The gold beam and nearby electrodes are fabricated on top of the membrane using e-beam lithography and thermal evaporation (Fig. 1(c)). The beam has length $l = 200 \mu\text{m}$, width $a = 0.24\mu\text{m}$ and thickness $t = 0.25\mu\text{m}$ (measured using AFM). In the last step the membrane is removed using electron cyclotron resonance plasma etching with an Ar/NF_3 gas mixture bombarding the back side of the sample. This leaves the gold beam suspended (Fig. 1(d)). Figure 1(e) is a micrograph showing a side view of the device.

To characterize the mechanical properties of the beam we employ two methods, namely, measurement of the resonance frequencies of the beam and measurement of the deflection due to an external force. Both methods lead to similar conclusions.

The equation of motion of the beam is given by:

$$\frac{\partial^2 y}{\partial x^2} - \zeta^2 l^2 \frac{\partial^4 y}{\partial x^4} = (\rho A/T) \frac{\partial^2 y}{\partial t^2} - f/T, \quad (1)$$

where $\zeta^2 = EAa^2/12Tl^2$, with E being Young's modulus, $A = at$ is the area of the beam's cross section, T is the tension, ρ is the mass density, and f is the density of external force. [9]. The clamping of the beam on both sides is taken into account using the boundary conditions $y(\pm l/2) = \frac{\partial y}{\partial x}(\pm l/2) = 0$.

The dimensionless parameter ζ indicates the relative effect of stiffness compared with tension on the dynamics of the beam. As we shall see below, $\zeta \ll 1$ in our case, therefore we expand the resonance frequencies of the system in powers of ζ using perturbation theory. To second order we find:

$$\nu_n = n\nu_0 [1 + 2\zeta + (4 + n^2\pi^2/2)\zeta^2], \quad (2)$$

where $\nu_0 = \sqrt{T/\rho A}/2l$. The equally spaced spectrum obtained for the case $\zeta = 0$ is the same as for a stiffness free beam with boundary conditions $y(\pm l/2) = 0$. Note that the terms that make the spectrum unequally spaced are of order $O(\zeta^2)$.

The resonance frequencies are measured *in-situ* using a commercial scanning electron microscope (SEM). The electron beam is focused on a point near the edge of the gold beam and the output signal from a photomultiplier (serving as a secondary electron detector) is monitored using a spectrum analyzer to detect mechanical displacement (see Fig. 2(a)). Note that this detection scheme is sensitive almost exclusively to motion in the plane of the sample.

Without applying any external excitation we find a pronounced peak near $\nu_1 = 176.5$ kHz associated with thermal excitation of the fundamental mode of the beam (see Fig. 2(b)). The thermal peaks of higher modes are too small to be detected, therefore we induce external excitation by applying an AC voltage to a nearby parallel electrode, separated from the beam by a gap of width $g = 5\mu\text{m}$. We find three higher modes with frequencies $\nu_2 = 354.4$ kHz, $\nu_3 = 529.8$ kHz, and $\nu_4 = 709.7$ kHz. The fact that the obtained spectrum is almost equally spaced indicates that $\zeta \ll 1$. Note, however, that drift in the position of the peaks occurring over time prevents us from making a precise estimation of ζ . Based on the uncertainty originated by this drift we place an upper bound of $\zeta < 0.015$.

Theoretically, the power of displacement noise near the center of the beam ($x = l/2$) around the fundamental frequency for the case $\zeta = 0$ is given by:

$$S_x(\omega) = \frac{\omega_0 k_B \Theta}{\pi Q m_{\text{eff}} \left[(\omega_0^2 - \omega^2)^2 + (\omega_0 \omega / Q)^2 \right]}, \quad (3)$$

where Q is the quality factor, $m_{\text{eff}} = \rho Al/2$ is the effective mass, $\omega = 2\pi\nu$ is angular frequency, and Θ is the temperature. Fitting the data in Fig. 2(b) with Eq. (3) yields

$Q = 1800$. The known parameters of the beam allow determination of the scaling factor translating the signal of the spectrum analyzer to actual displacement noise. Using this factor and the signal to noise ratio of the data in Fig. 2(b) we find the sensitivity of our displacement detection scheme to be $4 \times 10^{-13} \text{ m}/\sqrt{\text{Hz}}$. This value can be further enhanced by increasing the current of the electron beam. However, to minimize heating of the device due to electron bombardment we operate at a relatively low current of 100 pA. The energy absorbed by the sample depends on the penetration depth of electrons and on the thickness of the Au layer. For an acceleration voltage of 40 kV we estimate the heating power is of order 100 nW [10]. For thermal conductivity of 300 W/mK and the geometry of our device the temperature increase is $\approx 1\text{K}$.

To further establish our findings we study the deflection of the beam due to application of a uniform force. For this we apply D.C. voltage V between the beam and the nearby electrode. When the deflection is small compared to the distance between the beam and the electrode the force acting on the beam is approximately uniform. The expected deflection is found from the steady state solution of Eq. (1) with $f = \text{constant}$:

$$y(x) = \frac{fl^2}{2T} \left[\frac{1 - (2x/l)^2}{4} + \frac{\zeta [\cosh(x/\zeta l) - \cosh(1/2\zeta)]}{\sinh(1/2\zeta)} \right]. \quad (4)$$

Figure 3(a) shows a series of SEM pictures taken with $V = 0, 10, \dots, 70$ V. Using image processing we extract the shape of the beam in each picture, namely the experimental value of $y(x)$. Comparing the calculated $y(x)$ with experimental data using a least squared fit, we determine the parameter $\zeta = 0.014 \pm 0.007$, in agreement with the above mentioned estimate of ζ .

The value $\zeta = 0.01$ and the other known parameters allow estimating of Young's modulus $E = 8 \times 10^{10}$ N/m². This value shows reasonable agreement with previous measurements of E in thin films of evaporated gold using different methods ([11], [12], [13]).

Figure 3(b) shows the maximum displacement of the beam, namely $y(0)$, as a function of the voltage V . As expected, we find that this maximum displacement is proportional to V^2 . Using the value of $T = 5.8 \times 10^{-6}$ N found from the spectrum measurements we find that $f/V^2 = 4.6 \times 10^{-7}$ N/mV²

To study adhesion in our system we bring the beam and the nearby electrode to contact by introducing a pure liquid to the surface of the sample and employing the resultant capillary forces. During drying a thin layer of liquid is formed between the gold surfaces. The pressure inside the drop is lower than the pressure outside if the wetting angle is smaller than $\pi/2$, resulting in a net attractive force between the surfaces. We employ

DI water as an adhesive liquid due to its relatively high surface tension ($\cong 0.07 \text{ N/m}$ at room temperature).

Fig. 4 is a micrograph of the gold beam after drying the DI water from the surface of the sample. The length of the segment that adheres is $d = 67.8 \mu\text{m}$. The fact that adhesion between the beam and the nearby electrode persists after drying indicates that the total energy of the adhering system is lower than that of a straight free beam, which is merely metastable.

To estimate the total energy of the system we make two simplifying assumptions: (a) no stiffness, namely $\zeta = 0$ (the measured value $\zeta \simeq 0.01$ justifies this approximation); (b) no finite range interaction between the surfaces (the error due to this approximation is small due to the rapid decay of the interaction as a function of distance). Using the first assumption we find an expression for the elastic energy of the system

$$U_e = 2g^2T/(l-d). \quad (5)$$

The second assumption implies that the energy due to the surface-surface interaction is given by:

$$U_a = -st\gamma, \quad (6)$$

where γ is the energy of adhesion per unit area. The condition that the total energy of the system has a minimum implies:

$$\gamma = 2g^2T/t(l-d)^2. \quad (7)$$

Using the parameters of our sample we find $\gamma = 0.066 \text{ J/m}^2$. A similar value of 0.062 J/m^2 is obtained from another beam with a gap $g = 3 \mu\text{m}$.

What is expected theoretically? The Casimir force for small separation is reduced to the so-called non retarded van der Waals force [14]. In this regime the separation between the metallic surfaces is small compared to the characteristic wavelength of their absorption spectra and effects due to finite conductivity are strong. The interaction energy per unit area is given by

$$U = -A/12\pi d^2. \quad (8)$$

For the case of Au it was found that Eq. (8) is a good approximation for $d < 2 \text{ nm}$ and the Hamaker constant A is given by $A = 4.4 \times 10^{-19} \text{ J}$ [15]. This allows estimation of the adhesion energy by $\gamma = A/12\pi d_0^2$, where d_0 is the effective separation at contact. The nearest neighbor approximation for the case of atomically flat surfaces leads to $d_0 \approx 0.16 \text{ nm}$ [14], and therefore $\gamma \approx 0.4 \text{ J/m}^2$. For the case of metals it was shown that electron exchange interaction (giving rise to the so-called metallic bond) is expected to further enhance γ [16]. The enhancement factor, however, strongly depends on the twist angle between the contacting lattices. Previous measurements of γ of metals found values in the range of $0.4 - 4 \text{ J/m}^2$ [14].

There are two possible explanation for the factor of six discrepancy between our results and theory. The first is roughness existing on the surfaces in contact. From the measured value of γ , the calculated value of A , and the relation $\gamma = A/12\pi d_0^2$ we find an effective value for the separation between the surfaces within our sample of $d_0 \approx 0.4 \text{ nm}$. Note that this distance scale for d_0 is far smaller than can be resolved using SEM or AFM. Another possible cause for the discrepancy might be surface contamination that can strongly modify the adhesion energy even when this is from absorbed layers only a monolayer thick [14].

Apart from determining the adhesion energy, a central question is whether we can study the Casimir interaction at finite separation with such stiction experiments. In the immediate vicinity of the region of the beam that is in contact with the electrode, the separation between the beam and electrode is small. This gives rise to a strong Casimir interaction in this locate. In principle such attraction can cause additional bending of the beam, allowing thus determination of the magnitude of the attractive force using Eq. (1). To examine this possibility we estimate this additional bending assuming the attractive interaction is given by Eq. (8) with $A = 4.4 \times 10^{-19} \text{ J}$. We assume $\zeta = 0$ and solve Eq. (1) using the other known parameters of the beam. We find that the change in the separation between the beam and the electrode becomes comparable to the unperturbed one only when the separation is $< 1 \text{ nm}$. Resolving such a small effect is very difficult with a SEM but might be possible with transmission electron microscope imaging if charging does not become an issue. However, we find that the effect of stiffness on the shape of the beam is much stronger than the one due to Casimir attraction. Note, however, that observation of such Casimir induced bending may be easier using a stress free material with a low Young's modulus and employing a modified geometry.

As demonstrated by the present work, MEMS can provide ideal tools for characterizing stress in thin films as well as for studying adhesion forces. Future experiments with enhanced sensitivity should enable studies of the Casimir force at finite separations.

The authors are grateful to K. Schwab for his assistance in sample fabrication and Y. Buks for image processing of the SEM micrographs. This research was supported by the Rothschild Fellowship, the R. A. Millikan Fellowship at Caltech and DARPA MTO/MEMS under grant DABT63-98-1-0012.

[1] H. B. G. Casimir, Proc. Kon. Ned. Akad. Wetenschap **51**, 793 (1948).

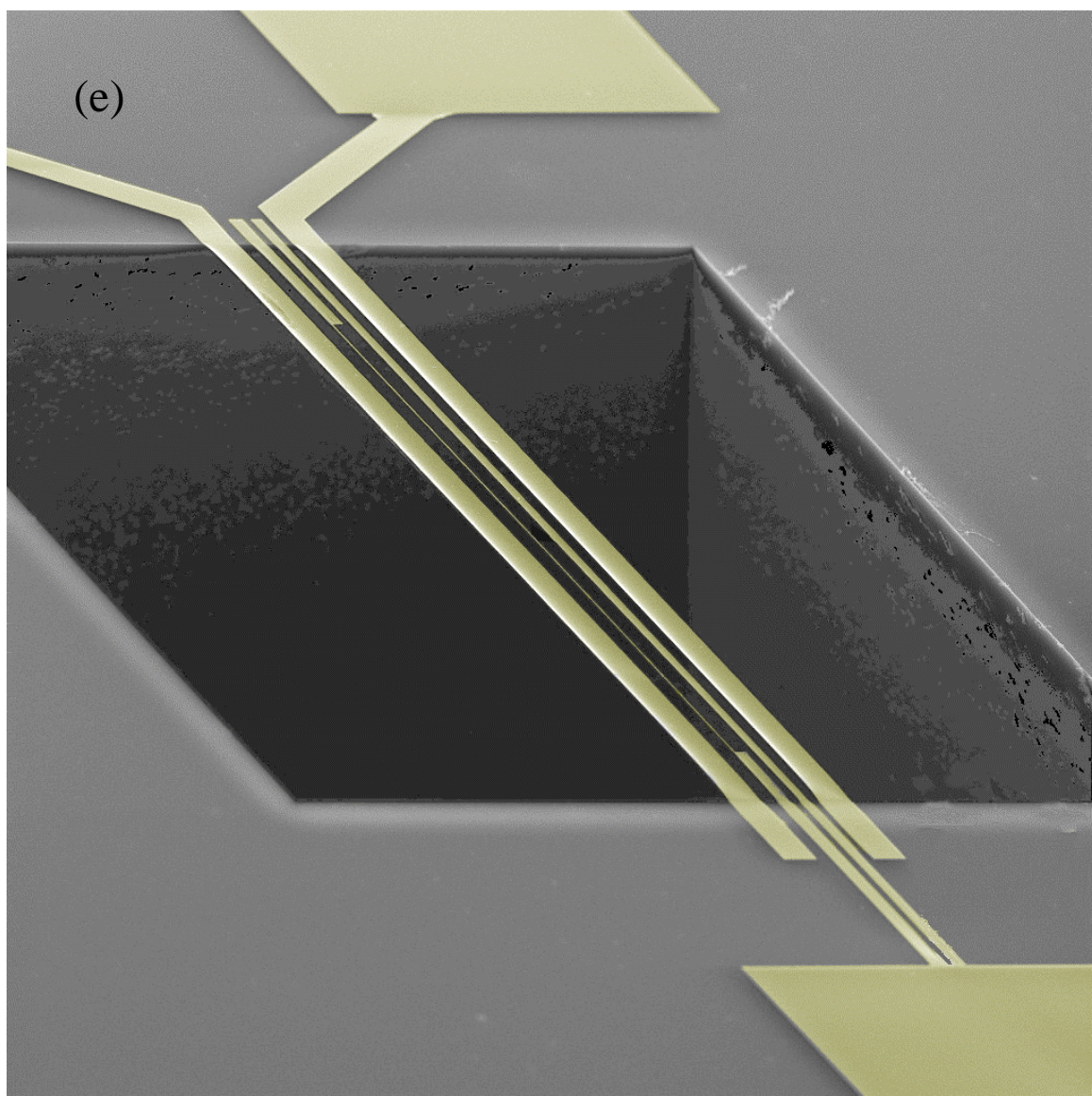
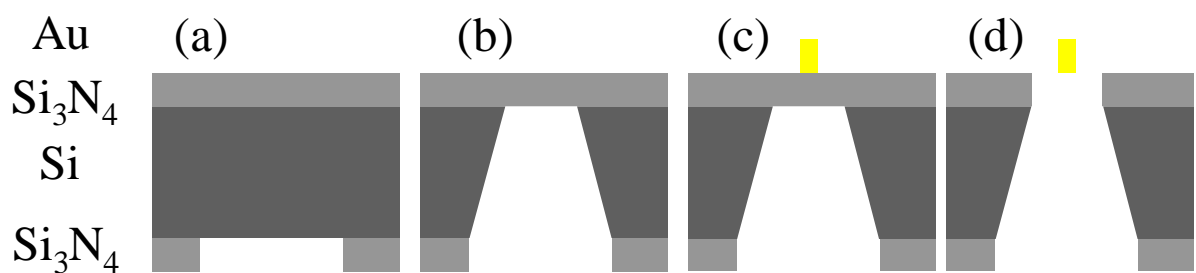
- [2] S. K. Lamoreaux, Am. J. Phys. **67**, 850 (1999).
- [3] S. K. Lamoreaux, Phys. Rev. Lett. **78**, 5 (1997); **81**, 5475 (1998).
- [4] U. Mohideen and A. Roy, Phys. Rev. Lett. **81**, 4549 (1998).
- [5] J. C. Long, H. W. Chan and J. C. Price, Nucl. Phys. B**539**, 23 (1999).
- [6] Niels Tas, Tonny Sonnenberg, Henri Jansen, Rob Legtenberg and Miko Elwenspoek, J. Micromech. Microeng. **6**, 385 (1996).
- [7] Roya Maboudian and Roger T. Howe, J. Vac. Sci. Technol. B**15**, 1 (1997).
- [8] F. Michael Serry, Dirk Walliser and Jordan Maclay, J. Appl. Phys. **84**, 2501 (1998).
- [9] L. D. Landau and E. M. Lifshitz, *theory of elasticity* (Pergamon 1986).
- [10] Ludwig Reimer, *Scanning Electron Microscopy* (Springer-Verlag 1985).
- [11] C. A. Neugebauer, J. Appl Phys. **31**, 1096 (1960).
- [12] A. Kinbara, S. Baba and N. Matuda, Thin Solid Films **141**, 229 (1986).
- [13] T. P. Weihs, S. Hong, J. C. Bravman and W. D. Nix, J. Mater. Res. **3**, 931 (1988).
- [14] J. N. Israelachvili, *Intermolecular and Surface Forces* (London: Academic 1992).
- [15] G. L. Klimchitskaya, U. Mohideen and V. M. Mostepanenko, quant-ph/0003093.
- [16] J. Ferrante and J. R. Smith, Phys. Rev. B**31**, 3427 (1985).

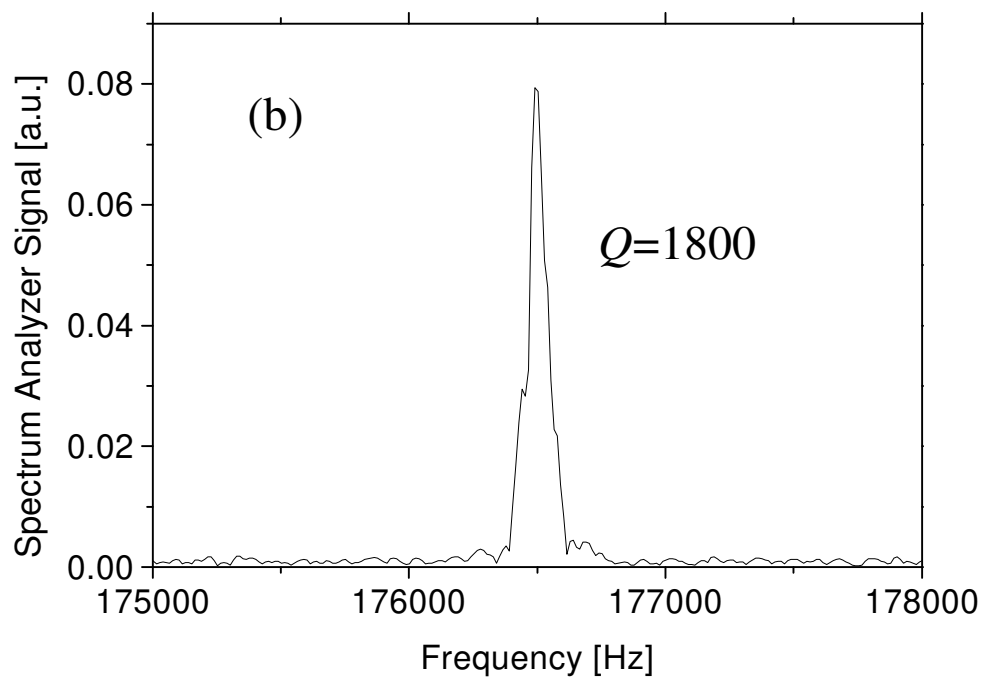
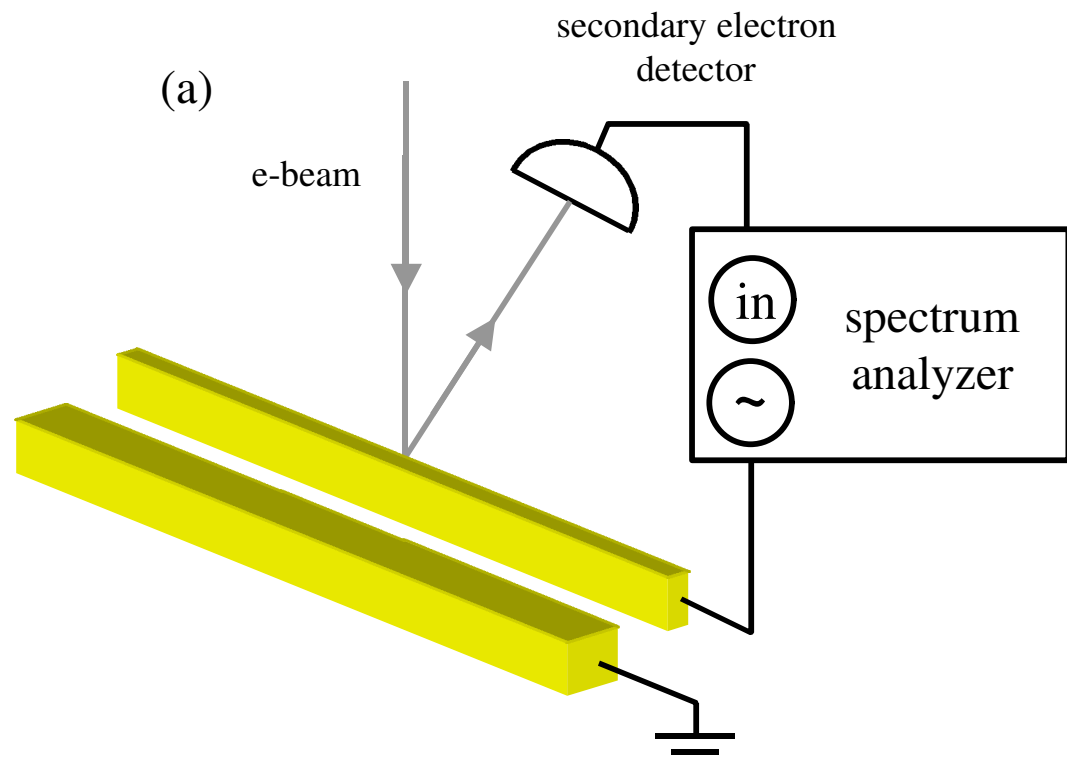
FIG. 1. The device is fabricated using bulk micromachining techniques. In steps (a) and (b) a suspended membrane of silicon nitride is formed. A gold beam is fabricated on top of the membrane (c) and the membrane is etched, leaving the beam suspended (d). Side view micrograph of the device is seen in (e).

FIG. 2. (a) The setup employed to detect the resonance frequencies of the beam. (b) peak in the displacement noise associated with thermal excitation of the fundamental mode.

FIG. 3. (a) deflection of the beam due to application of electrostatic force. (b) Displacement of the center of the beam as a function of applied voltage.

FIG. 4. Adhesion between the beam and a nearby electrode.





(a)

